ARTICLE

Thermal and light irradiation effect on the electrocatalytic performance of Hemoglobin modified Co_3O_4-g-C_3N_4 nanomaterials for oxygen evolution reaction

Received 00th January 20xx,
Accepted 00th January 20xx

DOI: 10.1039/x0xx00000x

Carlos Leal-Rodríguez,[†a] Daily Rodríguez-Padrón,[†a] Zeid A. Alothman,[*b] Manuel Cano,[*c] Juan J. Giner-Casares,[c] Mario J. Muñoz-Batista,[*d] Sameh M. Osman[b] and Rafael Luque[*a,b]

Oxygen evolution reaction (OER) plays a key role on the water splitting process and a high energy conversion efficiency is essential for the definitive advance of hydrogen-based technologies. Unfortunately, green and sustainable development of electrocatalysts for water oxidation is nowadays a real challenge. Herein, a successful mechanochemical method is proposed for the synthesis of a novel Hemoglobin (Hb) modified Co_3O_4/g-C_3N_4 composite nanomaterial. The controlled incorporation of Cobalt entities as well as the Hb functionalization, without affecting the g-C_3N_4 nanoarchitecture, was evaluated using different physicochemical techniques, such as X-ray diffraction, N_2-physisorption, scanning electron microscopy, UV-visible and X-ray photoelectronic spectroscopies. The beneficial effect of the resulting ternary bioconjugate together with the influence of the temperature and light irradiation were investigated by electrochemical analysis. Under 60 ºC and light exposition, this electrocatalyst requires an overpotential of 370 mV to deliver the current density of 10 mA·cm^{-2}, showing a Tafel slope of 66 mV·dec^{-1} and outstanding long-term stability for 600 OER cycles. This work paves the way for the controlled fabrication of multidimensional and multifunctional bio-electrocatalysts.

1. Introduction

The anthropogenic climate change together with the depletion of fossil fuels have motivated the rapid progress of hydrogen-based technologies, such as fuel cell and as carrier energy storage for harnessing renewable sources.[1–3] However, the future global application of these green and sustainable energy technologies requires the development of low-cost, efficient and durable electrocatalysts for electrochemical processes. For instance, the simplest method for solar to chemical energy conversion is water splitting, which involves the chemical breakdown of water into oxygen and hydrogen. These anodic and cathodic processes are known as oxygen (OER) and hydrogen (OER) evolution reactions, respectively. Although both need electrocatalysis, OER requires a higher theoretical overpotential of 1.23 V to provide a suitable current.[4–7]

Recently, transition-metal based electrocatalysts are emerging as an interesting alternative to the classical noble metals (e.g. Pt for HER and RuO_2/IrO_2 for OER). [8–11] Among all these chemical elements, Cobalt-based materials have been extensively investigated for water oxidation through different approaches, including oxides,[12,13] hydroxides,[14,15] chalcogenides,[16] carbides,[17] nitrides,[18] silicates,[19] phosphides,[20,21] alloys,[22,23] etc., to name only a few. Another interesting strategy is focused on Cobalt-supported onto conducting carbonaceous composite materials, such as graphene,[24] carbon nanotubes,[25,26] and its nitrogen-derivatives.[27,28] The latter approximations provide not only an enhanced OER electrocatalytic performance but also a substantial reduction of the total Cobalt content.

Inspired in all these approaches and considering that graphitic carbon nitride (g-C_3N_4) is a well-known metal-free electrocatalyst for HER and oxygen reduction reaction (ORR),[29–32] Wang et al.[33] and Zhu et al.[34] have recently reported two different Co_3O_4/g-C_3N_4 composite materials (i.e. Co_3O_4/g-C_3N_4 supported on N-doped graphene - 42.9%Co_3O_4@g-C_3N_4/NG- and Co_3O_4 supported on phosphorus-doped g-C_3N_4 -60%Co_3O_4/P-C_3N_4-, respectively) as efficient electrocatalysts for OER, demonstrating the enormous potential of this type of inorganic-organic hybrid combination. In this same direction, herein we propose a mechanochemical-assisted method to fabricate a novel multifunctional inorganic-organic biocomposite, which uses hemoglobin (Hb) as alternative material for reducing to 10 % the amount of Co_3O_4 into the Co_3O_4/g-C_3N_4 composite. Hb is a tetrameric redox protein formed by four polypeptide chains in which

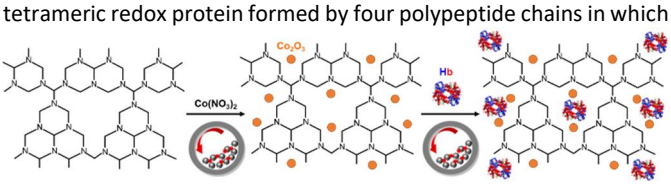

Scheme 1. Schematic representation of the proposed mechanochemical-assisted method. Molecules and NPs are not drawn to scale.

[a] Departamento de Química Orgánica, Universidad de Córdoba, Campus de Rabanales, Edificio Marie Curie (C-3), N. IV-A, Km 396, E14014, Córdoba, Spain. E-mail: rafael.luque@uco.es
[b] Department of Chemistry, College of Science, King Saud University, P.O. Box 2455, Riyadh, 11451, Saudi Arabia. E-mail: zaothman@ksu.edu.sa
[c] Departamento de Química Física y Termodinámica Aplicada, Instituto Universitario de Nanoquímica (IUNAN), Facultad de Ciencias, Universidad de Córdoba, Campus de Rabanales, Ed. Marie Curie, E-14071 Córdoba, Spain. E-mail: q82calum@uco.es
[d] Department of Chemical Engineering, Faculty of Sciences, University of Granada. Avda. Fuentenueva, s/n 18071, Granada, Spain. E-mail: mariomunoz@ugr.es
† Both authors contribute equally to the work.
Electronic Supplementary Information (ESI) available: XPS spectra and SEM-mapping images of 10%Co/g-C_3N_4 and 10%Co/g-C_3N_4-Hb samples are included. See DOI: 10.1039/x0xx00000x

each polypeptide domain encloses at least one iron active redox centre that provides both hierarchically structure and porous framework to the whole. This redox protein has been previously reported by Compton et al.[35] and Franco et al.[36] as an outstanding electrocatalytic biomaterial for ORR. Our characterization results demonstrate the beneficial effect between three components (i.e. g-C_3N_4, Co and Hb acting as porous network, catalytic transition-metal and tertiary structure, respectively) and provide insights on the influence of the temperature and light irradiation on its electrocatalytic performance, paving the way for the rational design and easy fabrication of multidimensional and multifunctional electrocatalysts with desired performances for hydrogen-based technologies.

2. Experimental

2.1. Synthesis of materials

The graphitic carbon nitride material (g-C_3N_4) was obtained using a previously optimized protocol.[37,38] The g-C_3N_4 (Fig. 1A) was obtained by calcination of melamine (Sigma-Aldrich) in a semi-closed crucible at 580 °C for 2 hours and using a heating rate of 5 °C min^{-1}. The obtained g-C_3N_4 was subsequently modified following a mechanochemical protocol to obtain ternary catalytic systems with minor amounts of Co_3O_4 and hemoglobin (Hb). The preparation of Co_3O_4 spices (pure reference and composites) was accomplished following a mechanochemical procedure at 350 rpm during 10 min. The binary samples (Co_3O_4/g-C_3N_4) was prepared employing the previously synthesized g-C_3N_4 and $[Co(NO_3)_2{\cdot}6H_2O]$ as cobalt precursor. Four materials, containing different Co concentrations (1, 2.5, 5 and 10 wt. %), were prepared. The syntheses were performed in a Retsch PM100 ball mill, using a 125 mL reaction chamber and eighteen 10 mm stainless steel balls and the solid precursor were oven-dried at 100 °C for 24 h, and finally calcined at 400 °C for 2h (5 °C/min). As well-demonstrated before, this protocol allows obtaining a dominant Co3O4 phase.[39] The final deposition of the Hb (Horse hemoglobin) was carried out using also a mechanochemical protocol at 200 rpm for 10 min (Retsch PM100 ball mill, 50 mL reaction chamber and eight 10 mm stainless steel balls).

The bioconjugate was prepared using 500 mg of the active support (Co_3O_4/g-C_3N_4) and 50 mg of Hb in 300 µL of NaH_2PO_4 buffer (pH=7).[40] Both, binary and ternary systems are displayed in Fig. 1. Sample names are X%Co/g-C_3N_4 for Co_3O_4/g-C_3N_4 composite materials and 10%Co/g-C_3N_4-Hb for the ternary systems modified with Hemoglobin.

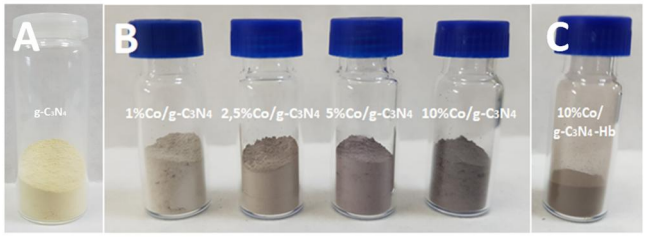

Fig. 1 Images of the different synthesized materials: (A) g-C_3N_4, (B) X%Co/g-C_3N_4 and (C) 10%Co/g-C_3N_4-Hb.

2.2. Characterization of materials

X-ray diffraction patterns were obtained using a Bruker D8 Advance Diffractometer with the LynxEye detector and acquired in a 2θ scan range from 10° to 70°. Phase identification was accomplished with Bruker Diffrac-plus Eva software. Brunauer–Emmett–Teller (BET) surface areas and porosity parameters were analyzed by N_2 physisorption measurements (Micromeritics ASAP 2000 equipment). The morphology and elemental composition of the samples were investigated by Scanning Electron Microscopy (SEM)/X-ray Energy Dispersive Spectra (EDX) analysis acquired in the JEOL-SEM JSM-7800 LV scanning microscope. XPS experiments were performed on 4×4 mm^2 pellets in an ultrahigh vacuum multipurpose surface analysis instrument SpecsTM. The samples were outgassed overnight in a pre-chamber under vacuum (10^{-6} Torr) and the measurements accomplished at room temperature using a conventional X-ray source with a Phoibos 150-MCD energy detector. XPS results were analyzed employing the XPS CASA software (version 2.3.15) and C 1s contribution utilized as energy calibration reference (284.6 eV). The UV-vis diffuse reflectance spectroscopy experiments were carried out using a LAMBDA 365 UV/Vis Spectrophotometer and the data processed employing the UV-Express software.

2.3. Electrochemical methods

Linear-sweep voltammetric (LSV) curves were recorded in a three-electrode electrochemical cell using a Potentiostat/Galvanostat instrument (AUTOLAB PGSTAT30). An oxygen-saturated aqueous solution of KOH 0.5 M was employed as electrolyte. Ag/AgCl and Pt foil were used as reference and counter electrodes, respectively. A glassy carbon (GC) disc of 5 mm in diameter (Pine Instruments Company) with two-dimensional geometry was used as working electrode, which was modified by drop-casting with 15 µL of an isopropanol:water 1:3 v/v dispersion of the different composite materials (4 mg/mL). All electrochemical experiments were scanned in the potential range between 0.00 V and 0.80 V vs Ag/AgCl, at a scan rate of 2 mV/s and a rotation rate of 1600 rpm. All potentials were referenced to RHE by adding a value of (0.205 + 0.059 x pH) V.[41,42] Illumination experiments were performed with an ORIEL LSH-7320 Alba Led Solar Simulator lamp using at output power of 1.0 mW/cm^2. The light source was placed 10 cm from the working electrode.

3. Results and discussion

Materials were prepared using a solvent-free (calcination/mechanochemistry) protocol (Scheme 1). Mechanochemical methods have broadly demonstrated their great applicability for nanomaterials design.[43] A milling-assisted deposition of cobalt oxide nanoparticles (Co_3O_4 NPs) on the surface of g-C_3N_4 material was successfully achieved. Fig. 2 shows representative TEM images of the 10%Co/g-C_3N_4 composite sample and its pure constituents (i.e. Co_3O_4 NPs and g-C_3N_4). Further modification of the obtained materials with hemoglobin was also efficiently performed by a mechanochemical protocol. Operating conditions detailed described in experimental section allow obtaining a dominant Co_3O_4 phase as well as the stable deposition of the bio-entities hemoglobin, both with potential in electro catalytic applications.[36] It is worth to highlight that solvent-free protocols and in particular mechanochemistry possesses an inherent sustainable character, avoiding the use of solvents and additional reagents in the synthesis of the materials. As well, the aforementioned methodology is highly

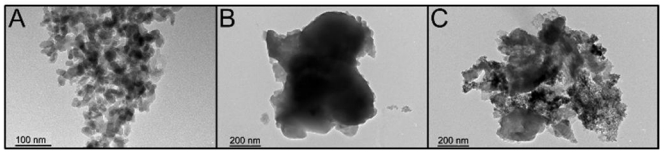

Fig. 2 Representative TEM images obtained for Co_3O_4 NPs (A), g-C_3N_4 (B) and 10%Co/g-C_3N_4 composite (C).

reproducible, versatile and simple, as well as allowing the preparation of a wide range of materials in short reaction times. Such advantages could motivate the scientific community to investigate the scalability and possible industrial applications of mechanochemistry.

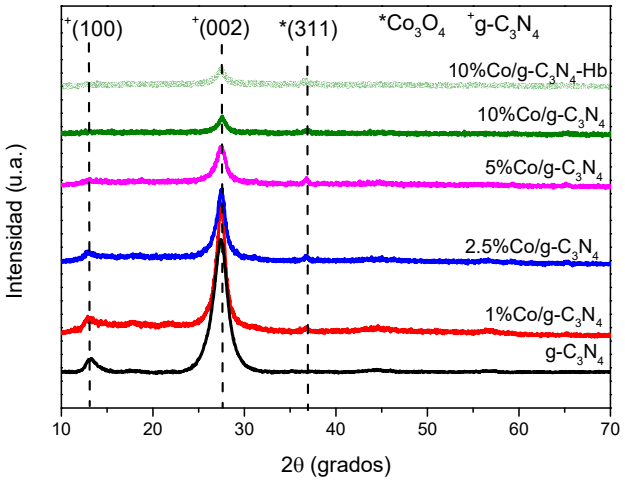

Fig. 3 XRD patterns of the prepared samples.

The crystalline structures of the synthesized carbon nitrile material and post-modified samples have been studied by X-ray diffraction analysis as shown in Fig. 3. Pure g-C_3N_4 as well as binary (XCo/g-C_3N_4) and ternary (Co/g-C_3N_4-Hb) composite samples showed as dominant contributions the two characteristic peaks of g-C_3N_4 that appear at 13.1° and 27.4°, associated with the crystallographic planes (100) and (002), respectively.[44–46] These data suggest that the crystalline structure of the g-C_3N_4 material has not been modified after the mechanochemical treatment or after the incorporation of Co and Hb spices. As well, it can be observed a small peak at 36.85°, associated with crystallographic plane (311), which was not found in the g-C_3N_4 sample. Such characteristic peak could be associated with Co_3O_4,[47] therefore confirming the successful formation of Co_3O_4 species and the effective deposition of cobalt counterpart on the g-C_3N_4 material.

Table 1. Textural properties of the synthesized materials.

Sample	Area BET (m^2/g)	Pore volume (cm^3/g)	Pore size (nm)
g-C_3N_4	25	0.10	20.1
1%Co/g-C_3N_4	25	0.10	19.8
2.5%Co/g-C_3N_4	24	0.09	19.3
5%Co/g-C_3N_4	23	0.09	18.9
10%Co/g-C_3N_4	19	0.08	18.5
10%Co/g-C_3N_4-Hb	19	0.08	18.5

The textural properties of the samples were determined by N_2 adsorption-desorption measurements and are shown in Table 1. The surface area of g-C_3N_4 material was found to be in good accordance with the reported values in the literature.[38,48–51] In addition, it was observed a decreasing trend of this property with the increment of the cobalt concentration. Even if such variation was small, it could indicate that cobalt oxide particles were partially blocking the pores of the g-C_3N_4 structure. On the other hand, it was observed that the incorporation of Hb had a negligible influence on the surface of the materials. In any case, the small differences detected after functionalization with Co and Hb strongly suggested that the textural properties are given by the main component (g-C_3N_4). The same conclusion can be deduced from the pore volume and the pore size data.

The optical properties of the synthesized materials were studied by UV-vis spectroscopy, as shown in Fig. 4. The pure g-C_3N_4 presented the expected profile with absorption from UV to visible light and a bandgap value of 2.7 eV, which is in accordance with the expected profile for graphitic carbon nitride materials.[50,51] Although some variation in the absorption edge of the composite samples (Co/g-C_3N_4) can be observed, the profile bellow 450 nm is dominated by the major g-C_3N_4 component, leading to band gap values in a range of 2.7-2.9 eV. Incorporation of the Co entities on the surface of the g-C_3N_4 drove to an enhancement of the abortion above 450 nm. The broad contribution situated at ~580 nm (inset) has been previously detected and associated with direct transitions at 1.45 eV, corresponding to O^{2-} to Co^{3+} excitation charge transfer.[52] The final modification with Hb described small differences in comparison to the composite support (10%Co_3O_4/g-C_3N_4), with negligible variations of the bandgap and a decrease of the absorption band generated by the Co_3O_4 counterpart. Such finding motivated the use of these materials as photo-electro-catalysts using sunlight-type illumination source.

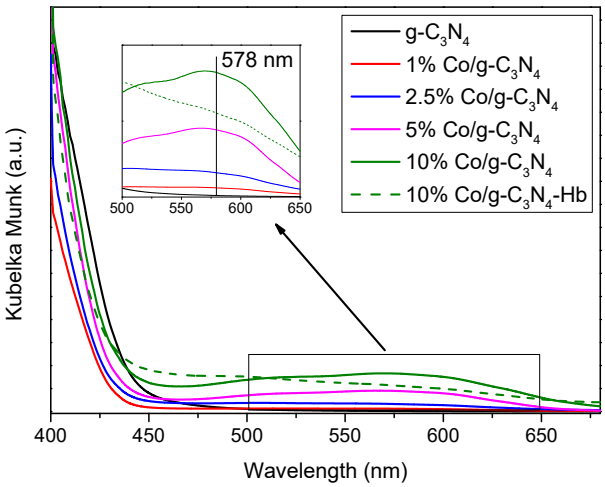

Fig. 4 UV-vis spectra of the synthesized samples.

The chemical properties of the samples were also studied by XPS measurements. The XPS regions of carbon 1*s* (C 1*s*), nitrogen 1*s* (N 1*s*), oxygen 1*s* (O 1*s*) and cobalt 2*p* (Co 2*p*) of 10% Co/g-C_3N_4 and 10% Co/g-C_3N_4-Hb samples were acquired, as shown in Fig. S1. It is important to note that very marked differences were detected in the C 1*s* region before and after the incorporation of Hb (Fig. S1A and S1E). In both samples, the C 1*s* XPS region showed three contributions corresponding to C-C, C-N and C-O, located around 284.6, 287.2 and 288.9 eV, respectively. The enhancement of the intensity of the C-C and C-O contributions in the 10% Co/g-C_3N_4-Hb sample can be exclusively attributed to the incorporation of the protein on the surface of the material.[53] In turn, in the sample 10% Co/g-C_3N_4-Hb, the peak located at 287.2 eV can be attributed to C-N bonds from structural moieties of g-C_3N_4,[37,45] as well as from peptide bonds in the protein chains. The incorporation of Hb modified the

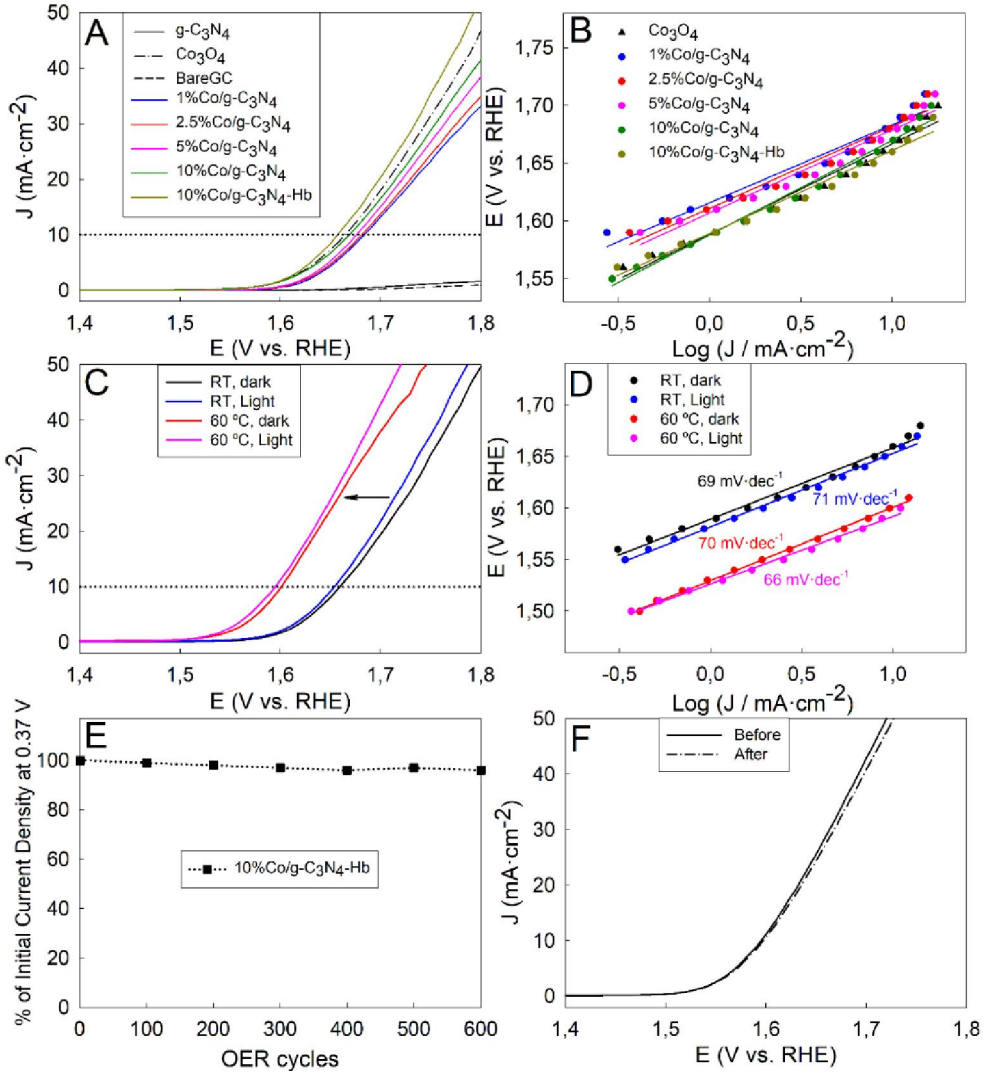

Fig. 5 (A) LSV curves of Bare-GC and GC modified with the different synthesized composites materials and its constituent part (i.e. g-C_3N_4 and Co_3O_4); (B) Tafel polarization plot obtained from (A); (C) LSV curves of the 10%Co/g-C_3N_4-Hb sample at different temperatures and illumination conditions; (D) Tafel polarization plot obtained from (C); (E) Long-term stability measurement of the 10%Co/g-C_3N_4-Hb sample performing 600 chronoamperometric OER cycles at a constant overpotential of 0.37 V; (F) LSV curves obtained before and after the durability test.

final XPS spectra of C 1*s*, by overlapping contributions, without considerable structural distortion of g-C_3N_4 sample.[37,45] The deconvolution of N 1*s* XPS region, in both materials showed the presence of three bands around 398.7, 399.5 and 400.8 eV, which were attributed to C-N-C bonds, NH residues and π excitation in g-C_3N_4 based materials, respectively (Fig. S1B and S1F). In particular, for the protein modified material, the peak located at 398.7 eV can also be associated with nitrogen from Hb peptide bonds.[53] On the other hand, the XPS region of O 1*s* exhibited two contributions in 530.9 and 532.0 eV, which can be assigned to O-Co/O-O and O-C bonds, respectively (Fig. S1C and S1G).[53,54] The increased intensity of the O-C band (Fig. S1G) may be related to the incorporation of the protein on the surface of the 10% Co/g-C_3N_4 material. Fig. S1D and S1H showed the Co 2*p* XPS region. The relative low variations of the binding energies from Co^{2+} to Co^{3+} are difficult to precisely identify cobalt chemical environments in cobalt oxides materials.[39,54] However, a dominant presence of Co_3O_4 is suggested based on the peak shapes of the spectra and the relatively low intensity of satellite peaks, characteristic of Co^{2+} in CoO species.[39,54,55]

The samples with the highest Co concentration were analysed by SEM-mapping. The obtained micrographs are shown in Fig. S2A-K. It could be observed the presence of carbon and nitrogen atoms, uniformly distributed. On the other hand, although some agglomerated areas are perceived in the oxygen and cobalt mapping images, it can be affirmed that cobalt oxide nanoparticles are homogeneously distributed over the surface of the g-C_3N_4 material. 10%Co/g-C_3N_4-Hb sample was also analysed by SEM-mapping. The obtained results are shown in Fig. S2F-K. In this case, the analysis revealed the presence of sulphur in the sample, most likely from the polypeptide chains of hemoglobin, particularly in methionine and cysteine amino acids.[56]

The electrocatalytic OER activity of the different synthesized composite materials and its constituent components were measured at room temperature and according to the detailed conditions in the experimental section. Fig. 5A shows their LSV plots, where a progressive increase of the OER activity of the different Co/g-C_3N_4 composites can be observed with the percentage of cobalt. Surprisingly, the 10%Co/g-C_3N_4 composite provides only a slight

lower OER activity than the 100%Co_3O_4 sample, indicating a favourable effect of the Co_3O_4 nanoparticles into the Co/g-C_3N_4 composite. In addition, the introduction of Hb into the 10%Co/g-C_3N_4 composite enhances significatively the resulting OER performance, which is even better than the one obtained for the 100%Co_3O_4 sample. This improvement can be attributed to the tertiary architecture of Hb with hierarchical structure and its iron active redox centre. Table 2 summarises some of the most important OER electrocatalytic parameters, which further confirm the observations above.

Table 2. OER electrocatalytic parameters obtained from Fig. 5A and 5B.

Sample	Onset potential (V)	Overpotential (mV) at 10 mV·cm^{-2}	Maximum current density (mV·cm^{-2})	Tafel slope (mV·dec^{-1})
BareGC	1.70	-	1.0	-
g-C_3N_4	1.68	-	2.0	-
Co_3O_4	1.54	430	47.5	78.0
1%Co/g-C_3N_4	1.58	470	33.0	67.4
2.5%Co/g-C_3N_4	1.59	460	32.0	70.9
5%Co/g-C_3N_4	1.56	450	37.0	71.8
10%Co/g-C_3N_4	1.54	440	35.0	81.8
10%Co/g-C_3N_4-Hb	1.54	420	50.0	71.9

Next, in order to improve the OER electrocatalytic performance of this tricomponent composite (i.e. 10%Co/g-C_3N_4-Hb), LSV measurements were carried out under light irradiation and at 60 ^oC (Fig. 5C). The finding shows that the temperature increase combined with the visible light-mediated photoexcitation improves significantly the OER electrocatalytic response, providing both cathodic shift of the onset potential (from 1.54 to 1.51 V) and increase of the maximum current density (from 50 to 80 mA·cm^{-2}), whilst the Tafel slopes maintained almost invariable as it can be observed in Fig. 5D. These results agree with the study reported by Zhang et al., who demonstrated an optimization of the HER activity of g-C_3N_4 through visible light irradiation.[29] They also suggested that g-C_3N_4 was a stable semiconductor, whose band-gap covered both the water reduction and water oxidation potentials. On the other hand, the comparison against others Co-based electrocatalysts reported in the literature,[7,57] our tricomponent composite material shows excellent properties as OER electrocatalyst, requiring an overpotential of 370 mV to deliver the current density of 10 mA·cm^{-2}, and with a Tafel slope of 66 mV·dec^{-1}. The latter values are quite similar that the ones reported recently for a 60%Co_3O_4/g-C_3N_4 modified GC electrode,[34] despite of using a 50 % higher amount of Co_3O_4. Finally, a durability test was carried out in order to assess the deterioration of its electrocatalytic performance after 600 chronoamperometric OER cycles. Fig. 5E shows that the percentage of the initial current density practically did not change after all these cycles. Fig. 5F shows the LSV curves obtained before and after the long-term stability study with the tricomponent composite material, further confirming the outstanding electrocatalytic behaviour for water oxidation.

Conclusions

We have demonstrated the excellent features provided by mechanochemical method for the synthesis of a novel multidimensional and multifunctional bionanomaterial. The incorporation of small amounts of cobalt, as well as the functionalization with hemoglobin, was evaluated using different techniques such as XRD, N_2-physisorption, SEM, UV-vis and XPS. As it was revealed by XRD and N_2 adsorption-desorption, neither the incorporation of Co_3O_4 nor Hb altered the nanoarchitecture of the g-C_3N_4. Similarly, XPS analysis confirmed the maintenance of the native-like structure of this redox protein into the biocomposite. Finally, electrochemical analysis confirmed the outstanding electrocatalytic performance for OER of the tricomponent bionanomaterial under 60 ^oC and light irradiation. This work opens the route for the development of novel composite biomaterials for diverse technological applications.

Conflicts of interest

There are no conflicts to declare.

Acknowledgements

Rafael Luque gratefully acknowledges Spanish Ministry of Economy and Competitiveness (MINECO) for funding project CTQ2016-78289-P, co-financed with European Regional Development Funds (FEDER). Daily Rodriguez-Padrón also gratefully acknowledges MINECO for providing research contract under the same project. Support from the MINECO of Spain is acknowledged through the MANA (CTQ2017-83961-R) and JEANS (CTQ2017-92264-EXP) projects. J.J.G.-C. acknowledges the MINECO for a "Ramon y Cajal" contract (#RyC-2014-14956). M.C. thanks to the FEDER and the Andalusian Government (Consejería de Economía, Conocimiento, Empresas y Universidades, Junta de Andalucía) of Spain for the financial support through UCO-1263193 project. The authors also thank Prof. Dr. J. M. Rodríguez-Mellado of the Department of Physical Chemistry and Applied Thermodynamics at the UCO for kind access to the rotating disk equipment. This work was supported by the Distinguished Scientist Fellowship Program (DSFP) at King Saud University, Riyadh, Saudi Arabia.

References

1 G. Brumfiel, *Nature*, 2003, **422**, 104.
2 N. Z. Muradov, T. N. Veziroğlu, *Int. J. Hydrogen Energy*, 2008, **33**, 6804–6839.
3 D. Schilter, *Nat. Rev. Chem.*, 2017, **1**, 0027.
4 X. Lu, W. -L. Yim, B. H. R. Suryanto, C. Zhao, *J. Am. Chem. Soc.*, 2015, **137**, 2901–2907.

5 R. van Putten, T. Wissink, T. Swinkels, E.A. Pidko, *Int. J. Hydrogen Energy*, 2019, **44**, 28533–28541.
6 I. Staffell, D. Scamman, A. Velazquez Abad, P. Balcombe, P. E. Dodds, P. Ekins, N. Shah, K. R. Ward, *Energy Environ. Sci.*, 2019, **12**, 463–491.
7 M. Tahir, L. Pan, F. Idrees, X. Zhang, L. Wang, J. -J. Zou, Z. L. Wang, *Nano Energy*, 2017, **37**, 136–157.
8 L. Najafi, S. Bellani, R. Oropesa-Nuñez, M. Prato, B. Martín-García, R. Brescia, F. Bonaccorso, *ACS Nano*, 2019, **13**, 3162–3176.
9 Y. Lian, H. Sun, X. Wang, P. Qi, Q. Mu, Y. Chen, J. Ye, X. Zhao, Z. Deng, Y. Peng, *Chem. Sci.*, 2019, **10**, 464–474.
10 B. Devi, R. R. Koner, A. Halder, *ACS Sustain. Chem. Eng.*, 2019, **7**, 2187–2199.
11 G. Yan, Y. Lian, Y. Gu, C. Yang, H. Sun, Q. Mu, Q. Li, W. Zhu, X. Zheng, M. Chen, J. Zhu, Z. Deng, Y. Peng, *ACS Catal.*, 2018, **8**, 10137–10147.
12 L. Wu, Q. Li, C.H. Wu, H. Zhu, A. Mendoza-Garcia, B. Shen, J. Guo, S. Sun, *J. Am. Chem. Soc.*, 2015, **137**, 7071–7074.
13 H. Xia, Z. Huang, C. Lv, C. Zhang, *ACS Catal.*, 2017, **7**, 8205–8213.
14 F. Lyu, Y. Bai, Q. Wang, L. Wang, X. Zhang, Y. Yin, *Dalt. Trans.*, 2017, **46**, 10545–10548.
15 P. T. Babar, A. C. Lokhande, B. S. Pawar, M. G. Gang, E. Jo, C. Go, M. P. Suryawanshi, S. M. Pawar, J. H. Kim, *Appl. Surf. Sci.*, 2018, **427**, 253–259.
16 K. Fan, H. Zou, Y. Lu, H. Chen, F. Li, J. Liu, L. Sun, L. Tong, M. F. Toney, M. Sui, J. Yu, *ACS Nano*, 2018, **12**, 12369–12379.
17 J. -H. Kim, K. Kawashima, B. R. Wygant, O. Mabayoje, Y. Liu, J. H. Wang, C. B. Mullins, *ACS Appl. Energy Mater.*, 2018, **1**, 5145–5150.
18 P. Chen, K. Xu, Y. Tong, X. Li, S. Tao, Z. Fang, W. Chu, X. Wu, C. Wu, *Inorg. Chem. Front.*, 2016, **3**, 236–242.
19 M. Cano, F. J. Garcia-Garcia, D. Rodríguez-Padrón, A. R. González-Elipe, J. J. Giner-Casares, R. Luque, *ChemCatChem*, 2019, **11**, 6111–6115.
20 X. Zhou, H. Gao, Y. Wang, Z. Liu, J. Lin, Y. Ding, *J. Mater. Chem. A*, 2018, **6**, 14939–14948.
21 J. Saha, D. R. Chowdhury, P. Jash, A. Paul, *Chem. A Eur. J.*, 2017, **23**, 12519–12526.
22 L. Bai, C. -S. Hsu, D. T. L. Alexander, H. M. Chen, X. Hu, *J. Am. Chem. Soc.*, 2019, **141**, 14190–14199.
23 W. Chen, Y. Zhang, G. Chen, Y. Zhou, X. Xiang, K. "Ken" Ostrikov, *ACS Sustain. Chem. Eng.*, 2019, **7**, 8255–8264.
24 X. Gong, A. Li, J. Wu, J. Wang, C. Wang, J. Wang, *Catal. Today*, 2019, doi:10.1016/j.cattod.2019.10.027.
25 Y. Liang, H. Wang, P. Diao, W. Chang, G. Hong, Y. Li, M. Gong, L. Xie, J. Zhou, J. Wang, T.Z. Regier, F. Wei, H. Dai, *J. Am. Chem. Soc.*, 2012, **134**, 15849–15857.
26 L. He, J. Liu, B. Hu, Y. Liu, B. Cui, D. Peng, Z. Zhang, S. Wu, B. Liu, *J. Power Sources*, 2019, **414**, 333–344.
27 Y. Zhang, W. Li, L. Lu, W. Song, C. Wang, L. Zhou, J. Liu, Y. Chen, H. Jin, Y. Zhang, *Electrochim. Acta*, 2018, **265**, 497–506.
28 Y. Liu, P. Dong, M. Li, H. Wu, C. Zhang, L. Han, Y. Zhang, *Front. Mater.*, 2019, **6**, 85.
29 J. Zhang, G. Zhang, X. Chen, S. Lin, L. Möhlmann, G. Dołęga, G. Lipner, M. Antonietti, S. Blechert, X. Wang, *Angew. Chemie Int. Ed.*, 2012, **51**, 3183–3187.
30 B. -J. Hwang, H. -C. Chen, F. -D. Mai, H. -Y. Tsai, C. -P. Yang, J. Rick, Y. -C. Liu, *Sci. Rep.*, 2015, **5**, 16263.
31 Z. Pei, J. Zhao, Y. Huang, Y. Huang, M. Zhu, Z. Wang, Z. Chen, C. Zhi, *J. Mater. Chem. A*, 2016, **4**, 12205–12211.
32 Z. Pei, Z. Tang, Z. Liu, Y. Huang, Y. Wang, H. Li, Q. Xue, M. Zhu, D. Tang, C. Zhi, *J. Mater. Chem. A*, 2018, **6**, 489–497.
33 Y. Wang, X. Yin, H. Shen, H. Jiang, J. Yu, Y. Zhang, D. Li, W. Li, J. Li, *Int. J. Hydrogen Energy,* 2018, **43**, 20687–20695.
34 M. Zhu, S. Yu, R. Ge, L. Feng, Y. Yu, Y. Li, W. Li, *ACS Appl. Energy Mater.*, 2019, **2**, 4718–4729.
35 S. V. Sokolov, L. Sepunaru, R. G. Compton, *Appl. Mater. Today*, 2017, **7**, 82–90.
36 A. Franco, M. Cano, J. J. Giner-Casares, E. Rodríguez-Castellón, R. Luque, A. R. Puente-Santiago, *Chem. Commun.,* 2019, **55**, 4671–4674.
37 M. J. Muñoz-Batista, O. Fontelles-Carceller, A. Kubacka, M. Fernández-García, *Appl. Catal. B Environ.*, 2017, **203**, 663–672.
38 M. J. Muñoz-Batista, O. Fontelles-Carceller, M. Ferrer, M. Fernández-García, A. Kubacka, *Appl. Catal. B Environ*., 2016, **183**, 86–95.
39 A. Pineda, M. Ojeda, A. A. Romero, A. M. Balu, R. Luque, *Microporous Mesoporous Mater*., 2018, **272**, 129–136.
40 D. Rodriguez-Padrón, A. R. Puente-Santiago, A. M. Balu, A. A. Romero, R. Luque, *Chem. Commun*., 2017, **53**, 7635–7637.
41 D. Alba-Molina, A. R. Puente Santiago, J. J. Giner-Casares, M. T. Martín-Romero, L. Camacho, R. Luque, M. Cano, *J. Phys. Chem. C*, 2019, **123**, 9807–9812.
42 D. Alba-Molina, A. R. Puente Santiago, J. J. Giner-Casares, E. Rodríguez-Castellón, M. T. Martín-Romero, L. Camacho, R. Luque, M. Cano, *J. Mater. Chem. A*, 2019, **7**, 20425–20434.
43 M. J. Muñoz-Batista, D. Rodriguez-Padron, A.R. Puente-Santiago, R. Luque, *ACS Sustain. Chem. Eng*., 2018, **6**, 9530–9544.
44 X. Wang, K. Maeda, A. Thomas, K. Takanabe, G. Xin, J. M. Carlsson, K. Domen, M. Antonietti, *Nat. Mater.*, 2009, **8**, 76–80.
45 M. J. Muñoz-Batista, M. A. Nasalevich, T. J. Savenije, F. Kapteijn, J. Gascon, A. Kubacka, M. Fernández-García, *Appl. Catal. B Environ.*, 2015, **176–177**, 687–698.
46 M. J. Muñoz-Batista, M. Fernández-García, A. Kubacka, *Appl. Catal. B Environ.*, 2015, **164**, 261–270.
47 H. Yang, Y. Hu, X. Zhang, G. Qiu, *Mater. Lett.*, 2004, **58**, 387–389.
48 J. Xu, H. T. Wu, X. Wang, B. Xue, Y. X. Li, Y. Cao, *Phys. Chem. Chem. Phys.*, 2013, **15**, 4510–4517.
49 M. Wu, Y. Gong, T. Nie, J. Zhang, R. Wang, H. Wang, B. He, *J. Mater. Chem. A*, 2019, **7**, 5324–5332.
50 K. Cerdan, W. Ouyang, J. C. Colmenares, M. J. Muñoz-Batista, R. Luque, A. M. Balu, *Chem. Eng. Sci.*, 2019, **194**, 78–84.
51 M. J. Muñoz-Batista, D. Rodríguez-Padrón, A. R. Puente-Santiago, A. Kubacka, R. Luque, M. Fernández-García, *ChemPhotoChem*, 2018, **2**, 870–877.
52 P. Suyana, P. Ganguly, B. N. Nair, A. P. Mohamed, K. G. K. Warrier, U. S. Hareesh, *Environ. Sci.: Nano*, 2017, **4**, 212–221.
53 D. Rodríguez-Padrón, A. R. Puente-Santiago, A. Caballero, A. Benítez, A. M. Balu, A. A. Romero, R. Luque, *J. Mater. Chem. A*, 2017, **5**, 16404–16411.
54 M. C. Biesinger, B. P. Payne, A. P. Grosvenor, L. W. M. Lau, A. R. Gerson, R. S. C. Smart, *Appl. Surf. Sci.*, 2011, **257**, 2717–2730.
55 M. Pal, R. Rakshit, A. K. Singh, K. Mandal, *Energy*, 2016, **103**, 481–486.
56 C. Jacob, G. I. Giles, N. M. Giles, H. Sies, *Angew. Chemie Int. Ed.*, 2003, **42**, 4742–4758.
57 H. Zhong, C. Campos-Roldán, Y. Zhao, S. Zhang, Y. Feng, N. Alonso-Vante, *Catalysts*, 2018, **8**, 559.

